Journal of Applied Physics

Moving photoacoustic sources: Acoustic waveforms in one, two, and three dimensions and application to trace gas detection

Cite as: J. Appl. Phys. **125**, 060902 (2019); https://doi.org/10.1063/1.5080267
Submitted: 06 November 2018 . Accepted: 19 January 2019 . Published Online: 13 February 2019

Wenyu Bai, and Gerald J. Diebold

AIP Publishing

Journal of Applied Physics PERSPECTIVE scitation.org/journal/jap

Moving photoacoustic sources: Acoustic waveforms in one, two, and three dimensions and application to trace gas detection

Cite as: J. Appl. Phys. **125**, 060902 (2019); doi: 10.1063/1.5080267
Submitted: 6 November 2018 · Accepted: 19 January 2019 ·
Published Online: 13 February 2019

View Online Export Citation CrossMark

Wenyu Bai and Gerald J. Diebold[a)]

AFFILIATIONS

Department of Chemistry, Brown University, Providence, Rhode Island 02912, USA

[a)]Gerald_Diebold@Brown.edu

ABSTRACT

The photoacoustic effect is governed by a wave equation with a source term proportional to the time derivative of the optical heat deposition per unit volume and time. Although the typical configuration for generation of the photoacoustic effect makes use of pulsed or amplitude modulated optical beams, the form of the source term in the wave equation indicates that a continuous optical source moving in an absorbing medium is capable of sound generation as well. Here, the properties of simple sources moving in one, two, and three space dimensions are reviewed. The salient feature of sources moving in one-dimension at sound speed is that the amplitude of the acoustic wave increases with time without bound according to linear acoustics. Two schemes, one in the time-domain and the other in the frequency-domain, that take advantage of this principle for increasing the sensitivity of trace gas detection are reviewed.

I. INTRODUCTION

The photoacoustic effect, first reported by Bell[1] in 1881, refers to the generation of sound by absorption of light. In gases and liquids, the initial step in the process following optical excitation of the internal degrees of freedom of a molecule is collisional relaxation of the absorbed energy to generate a heating, which in almost every substance results in an expansion. As the expansion is a mechanical motion, the result is the launching of a sound wave, which can be recorded by a microphone, a hydrophone, or by other standard acoustic transducers. In the case of solids in contact with a gas,[2] a somewhat different mechanism is operative. Some of the heat generated by the modulated optical radiation on the surface of the solid is transmitted to a thin gas layer in contact with the surface that acts as a moving piston, launching sound outwardly from the solid. The photoacoustic effect that takes place on the surface of a solid is frequently used for recording the absorption spectrum of the solid.

The photoacoustic effect has seen wide application to trace gas detection,[3,4] where almost universally an intensity modulated laser tuned to the absorption of the species of interest is directed into a resonator equipped with a sensitive microphone.[5,6] A trace gas detection method based on a resonant transducer[7] has recently been introduced whose sensitivity is governed by the high quality factor of a miniature piezoelectric tuning fork. Pulsed laser excitation of gases[8] in a resonator where the laser operates at the resonance frequency of a cylindrical resonator has shown excellent sensitivity as well. In fluids[9,10] and biological[11] samples, the preferred method of excitation makes use of a pulsed laser together with a wide bandwidth transducer.

It can be shown that motion of an optical source in an absorbing medium can produce sound as well. Both theoretical study and experimental generation of the photoacoustic effect by moving optical sources have been explored several decades ago by Soviet researchers including Bozhkov,[12–15] Bunkin,[12–14,16] and Kolomenskii[14,15] as well as researchers in the United States[17] who noted the Doppler effect from moving amplitude modulated sources and determined details of the spatial patterns of the emitted acoustic waves. Unfortunately, due to the proposed application for submarine communication, the bulk of the published work[12–16,18–21] by the Soviet

researchers has focused on the problem of a moving laser beam directed at the interface between a transparent gas and an absorbing liquid, which complicates the understanding of the form of the sound patterns in space and results in cumbersome mathematical expressions. That is, the character of waves emitted from simple sources is obscured by inclusion of amplitude modulation and the presence of a strongly reflecting boundary.

Here, we review solutions to the wave equation for the photoacoustic effect generated by sources moving in weakly absorbing fluids and describe experimental work that makes use of the moving source effect for trace gas detection. Section II gives the governing equations for photoacoustic process in fluids. Acoustic waveforms resulting from moving sources in different geometries are described and compared in Sec. III with a focus on rectilinear motion. Section IV describes a superposition approach to obtaining the waveform based on a previously published theorem for mapping, giving a new perspective for the process of sound generation by source motion. In Sec. V, applications of the moving source effect for the detection of trace gases are described. Section VI gives a summary of the work reviewed in the paper and describes the contrast between the acoustic waves generated by uniformly moving heat sources and the fields from uniformly moving electric charges.

II. GOVERNING EQUATIONS

The excitation and propagation of photoacoustic waves in an isotropic, homogeneous, and inviscid fluid medium are governed by the following linearized conservation equations:

$$\frac{\partial \rho}{\partial t} + \rho_0 \nabla \cdot \mathbf{u} = 0, \tag{1a}$$

$$\rho_0 \frac{\partial \mathbf{u}}{\partial t} + \nabla p = 0, \tag{1b}$$

$$\frac{\partial p_1}{\partial t} - c^2 \frac{\partial \rho_1}{\partial t} = \frac{\beta c^2}{C_p} H, \tag{1c}$$

where variables with the subscript 0 indicate hydrostatic quantities, while others refer to perturbation, ρ is the density, $\mathbf{u} = (u_x, u_y, u_z)$ is the particle velocity vector, p is the pressure, β is the thermal expansion coefficient, c is the sound speed, C_p is the isobaric specific heat capacity, and H is the deposited energy per unit volume and time. Equations (1a), (1b), and (1c) describe the conservation of mass, momentum, and energy, respectively.[22] Since pressure is the most easily recorded acoustic parameter, it is often preferential to decouple the five unknowns in Eq. (1) to give the governing equation for pressure as

$$\left(\nabla^2 - \frac{1}{c^2}\frac{\partial^2}{\partial t^2}\right) p = -\frac{\beta}{C_p}\frac{\partial H}{\partial t}, \tag{2}$$

when heat conduction can be neglected. Frequently, it is more convenient to determine the photoacoustic pressure by solving the wave equation[23] for the velocity potential φ given by

$$\left(\nabla^2 - \frac{1}{c^2}\frac{\partial^2}{\partial t^2}\right) \varphi = \frac{\beta}{\rho_0 C_p} H(\mathbf{x}, t) \tag{3}$$

rather than working with the wave equation for pressure as the forcing function for the former has the heating function itself instead of its time derivative. Additionally, the initial conditions for φ can be clearly determined in most cases by setting φ and $\partial\varphi/\partial t$ to be zero, while the quantity $\partial p/\partial t$ at the initial time is commonly obscure.[24]

Following determination of the potential it is straightforward to calculate the photoacoustic pressure p and velocity $\mathbf{u}$ using

$$p = -\rho_0 \frac{\partial \varphi}{\partial t} \text{ and } \mathbf{u} = \nabla \varphi. \tag{4}$$

III. ACOUSTIC WAVEFORMS IN DIFFERENT GEOMETRIES

A. Motion in one dimension

In one dimension, the velocity potential can be calculated via the D'Alembert formula,[25] yielding

$$\varphi = \frac{1}{2}\varphi_0(z - ct) + \frac{1}{2}\varphi_0(z + ct) + \frac{1}{2c}\int_{z-ct}^{z+ct} \varphi_1(\xi) d\xi - \frac{\beta c}{2\rho C_P}\int_0^t dt' \int_{z-c(t-t')}^{z+c(t-t')} H(z', t') dz', \tag{5}$$

where φ_0 and φ_1 are the initial conditions for the potential and its first time derivative, respectively. Assuming no perturbation exists before the initiation of the optical source, φ_0 and φ_1 are thus taken to be zero.

Consider an optical source moving along a one-dimensional channel with a speed v, where the absorbing medium with an absorption coefficient $\bar{\alpha}$ is optically thin.[24] The heating function for the source can be written as

$$H(z, t) = \frac{\bar{\alpha} F_0}{\sqrt{\pi}\theta} e^{-(t - z/v)^2/\theta^2}, \tag{6}$$

where F_0 is the laser fluence representing the energy received per unit irradiated area and θ is the temporal beam width parameter.

Substitution of Eq. (6) into Eq. (5) yields the corresponding velocity potential, which after time differentiation and multiplication with ρ_0 gives the photoacoustic pressure as

$$p = \frac{\bar{\alpha}\beta F_0 c v}{4 C_p}\left[\frac{\mathrm{erf}\left(\frac{t - z/c}{M\theta}\right) - \mathrm{erf}\left(\frac{t - z/v}{\theta}\right)}{1 - M} + \frac{\mathrm{erf}\left(\frac{t + z/c}{M\theta}\right) + \mathrm{erf}\left(\frac{t - z/v}{\theta}\right)}{1 + M}\right], \tag{7}$$

where M is the Mach number defined as v/c. The salient feature of the solution given by Eq. (7) as can be seen in the inset of Fig. 1(a) is that the initial motion launches compressive waves moving with the sound speed in both the positive and negative z directions at the time the motion begins. This feature is found solely as a consequence of initiation of

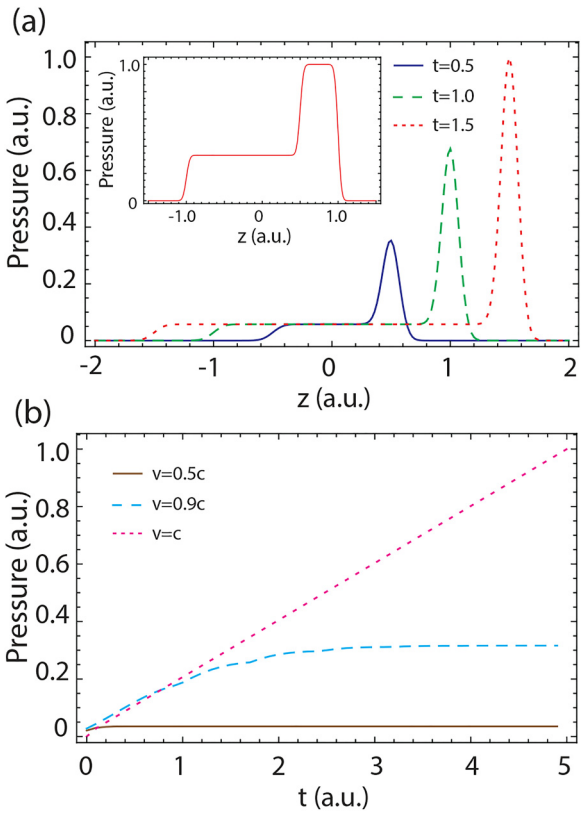

FIG. 1. (a) Photoacoustic pressure versus coordinate for different times as a Gaussian source moves at the sound speed in the one dimensional geometry starting from $z = 0$. Inset: photoacoustic pressure at $t = 1$ for the same Gaussian source moving at half of the sound speed. The parameters for the waveforms in the inset are $\theta = 0.1$, $c = 1$, and $v = 0.5$. The step-like character of the waveform is a result of instantaneous initiation of the motion of the source. The width of the first part of the right going pulse increases as $(c - v)t$. (b) The maximum pressure versus traveling time of the source for different speeds of motion. It is found that the linear amplification of the pressure amplitude occurs only for a source moving at the sound speed.

motion and is found in problems with symmetry in all three dimensions. The amplitude of the right-going compressive component of the wave that precedes the optical beam in space can be seen to exceed that of the left-going wave.

When the speed of the optical source approaches the sound speed, the photoacoustic pressure can be found by taking the limit of Eq. (7) as v approaches c to give

$$p = \frac{\bar{\alpha}\beta F_0 c^2}{2\sqrt{\pi} C_p}\left\{\left(\frac{t}{\theta}\right)e^{-(t-z/c)^2/\theta^2} + \frac{\sqrt{\pi}}{4}\left[\operatorname{erf}\left(\frac{t-z/c}{\theta}\right) + \operatorname{erf}\left(\frac{t+z/c}{\theta}\right)\right]\right\}. \tag{8}$$

As can be seen from Fig. 1(a), the remarkable feature of this solution is that the leading edge of the wave increases linearly in time *without bound*—at least according to linear acoustics. A deeper analysis[26] using the equations of nonlinear acoustics shows that the simple linear dependence of pressure on time given in Eq. (8) no longer obtains for large amplitude waves where the fluctuations in the density or pressure become comparable to their ambient values; as well, a change in time profile of the wave is found. It is noted that such amplification only occurs when the source moves at the sound speed. It can be seen from Fig. 1(b) that when the source moves at half of the sound speed, the pressure amplitude levels out rapidly with a relatively small amplitude. In Sec. V, two schemes of trace gas detection are introduced based on the rise of the photoacoustic pressure with time.

B. Motion in two dimensions

Consider the photoacoustic effect from a vertically directed delta function optical source (i.e., a delta function pulse parallel to the z axis) moving away from the origin along the x axis with a speed v, which is taken to be lower than the sound speed. The heating function for such a source can be written as

$$H = P_L \delta(x - vt)\delta(y), \tag{9}$$

where P_L is the absorbed power per unit length. The Poisson solution[25] to the wave equation for the velocity potential in two dimensions is given by

$$\begin{aligned}\varphi &= -\frac{\beta c}{2\pi\rho_0 C_P}\int_0^t dt' \int_A \frac{H(\mathbf{x}', t')}{\sqrt{c^2(t-t')^2 - |\mathbf{x} - \mathbf{x}'|^2}} d\mathbf{x}' \\ &= -\frac{\beta P_L}{2\pi\rho_0 C_P}\int_0^t \frac{1}{\sqrt{(t'-tr_1)(t'-tr_2)}} dt',\end{aligned} \tag{10}$$

where A refers to the volume subject to the causal condition $|\mathbf{x} - \mathbf{x}'| < c(t - t')$, which determines the two causal times t_{r1} and t_{r2} as given by

$$t_{r1} = \frac{c^2 t - vx - \sqrt{c^2\left[(x-vt)^2 + y^2\right] - v^2 y^2}}{c^2 - v^2},$$
$$t_{r2} = \frac{c^2 t - vx + \sqrt{c^2\left[(x-vt)^2 + y^2\right] - v^2 y^2}}{c^2 - v^2}.$$

It is noted that the second integral above has to be evaluated at some subinterval of $[0, t]$ to guarantee causality. The retarded time[29] is taken as t_{r1}, and thus the integration interval can be replaced with $[0, t_{r1}]$, which gives

$$\varphi = -\frac{P_L \beta}{\pi\rho C_P\sqrt{1 - M^2}} \operatorname{arctanh}\left(\sqrt{\frac{ct - Mx - \Delta}{ct - Mx + \Delta}}\right), \tag{11}$$

where $\Delta = \sqrt{(x - vt)^2 + (1 - M^2)y^2}$. The photoacoustic pressure is found through the use of Eq. (4) to be

$$p = \frac{P_L \beta c}{2\pi C_P}\frac{x^2 + y^2 - xvt}{\sqrt{c^2 t^2 - x^2 - y^2}\left\{(x - vt)^2 + (1 - M^2)y^2\right\}}. \tag{12}$$

Figure 2 shows the distribution of the photoacoustic pressure for the moving line source. The outmost compressive layer results from the abrupt initiation of the optical heating, inside of which is a compressive peak followed by a rarefaction. The pressure distribution along the x axis is shown in Fig. 2(b). The slow decay of the acoustic pressure to the baseline following the rarefaction pulse is characteristic of two-dimensional waves, as noted by Landau and Lifshitz in Ref. 27.

To find out how the pressure increases with time as the source moves at the sound speed, a moving source with a Gaussian heating function is considered which is written as

$$H(\vec{\mathbf{r}}, t) = \frac{\bar{\alpha}P}{2\pi\sigma^2} e^{-\frac{(x-ct)^2+y^2}{\sigma^2}}, \tag{13}$$

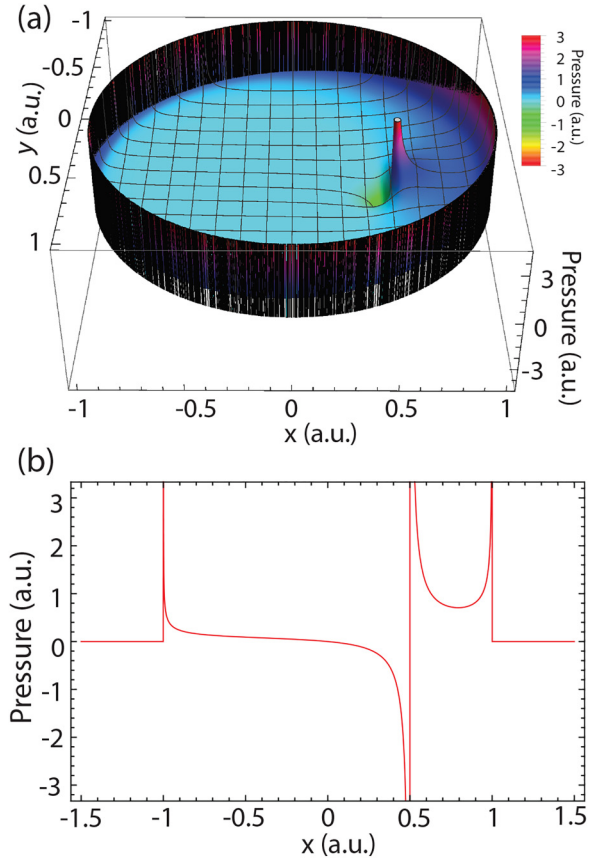

FIG. 2. Photoacoustic pressure from a delta source moving at half of the sound speed in a two dimensional geometry. (a) Distribution of the pressure on the xy plane at $t = 1$. The outer cylindrical fence originates from the abrupt initiation of the source at $t = 0$, which corresponds to the singularity shown in the denominator of Eq. (12). The pressure is truncated between −3 and 3 to permit visualization of the fine features of the wave within the causal region. (b) The pressure distribution along the x axis. A trailing tail extending from the rarefaction to the edge of the causal region exists, which is a typical feature of two-dimensional cylindrical waves. What appears to be structure in the circular fences here and in the following figure is an artefact of the plotting.

where P is the laser power and σ is a spatial width parameter of the laser beam. A finite difference numerical scheme is used to evaluate the temporal evolution of the pressure amplitude at the optical source. It is found in Sec. III C that compared with the linear rise of pressure with time in the one-dimensional geometry, the amplification effect for the two-dimensional wave is weakened, which is mainly due to the geometric divergence of the two-dimensional cylindrical waves.

For the case of supersonic motion, it is advantageous to write the velocity potential and pressure in a piecewise function form, that is, the area of interest is divided into two parts which include a causal circular region and a Mach cone as shown in Sec. III C. In region I, only t_{r1} is positive. We can therefore replace the integral interval $[0, t]$ in Eq. (10) with $[0, t_{r1}]$. Equation (10) can thus be evaluated to give

$$\varphi = -\frac{P_L\beta}{2\pi\rho_0 C_P\sqrt{1-M^2}}\left[\frac{\pi}{2} + \operatorname{arctanh}\left(\sqrt{\frac{ct-Mx-\Delta}{ct-Mx+\Delta}}\right)\right]. \tag{14}$$

While in region II, two retarded times exist and the integration needs to be conducted from t_{r2} to t_{r1} giving

$$\varphi = -\frac{P_L\beta c}{2\rho_0 C_P(v^2-c^2)},$$

which is a constant in time. The pressure can then be evaluated as

$$p = \frac{P_L\beta c}{2\pi C_P}\begin{cases} \frac{x^2+y^2-xvt}{\sqrt{c^2t^2-x^2-y^2\{(x-vt)^2+M^2y^2\}}} & \text{region I,} \\ 0 & \text{region II.} \end{cases} \tag{15}$$

What is surprising here is that within region II, the region inside the Mach cone, the pressure vanishes, which is a result of destructive interference between the waves arriving from two retarded times. It should be noted that Eq. (15) describes only the pressure within the corresponding domains excluding the domain boundary. Actually, on the boundaries of both regions, the pressure always goes to infinity. For region I, the infinity comes from the term $c^2t^2 - x^2 - y^2$ in the denominator of the pressure expression. For region II, this infinity results from the sharp discontinuity of the velocity potential across the boundary, which, after time differentiation, generates a delta function on the Mach cone boundary.

C. Motion in three dimensions

The Kirchhoff formula for the solution of the wave equation in three dimensions is well-known from the electromagnetic theory.[28,29] As given in Refs. 25 and 28, the solution for the velocity potential with homogeneous initial conditions can be written as

$$\varphi = -\frac{\beta c}{4\pi\rho_0 C_P}\int \frac{H(\mathbf{x}', t-\frac{|\mathbf{x}-\mathbf{x}'|}{c})}{|\mathbf{x}-\mathbf{x}'|}d\mathbf{x}', \tag{16}$$

where the integration is restricted to the domain $|\mathbf{x} - \mathbf{x}'| < ct$.

For a point source moving along the z axis with a constant speed, the corresponding heating function can be written as

$$H(\vec{\mathbf{r}}, t) = P_0\delta(z - vt)\delta(x)\delta(y),$$

where P_0 is the optical power delivered into the fluid. The velocity potential can thus be evaluated as

$$\varphi = -\left(\frac{\beta P_0}{4\pi\rho_0 C_P}\right)\frac{u(t_r)}{\sqrt{(z - vt)^2 + (x^2 + y^2)(1 - M^2)}}, \tag{17}$$

where $u(t)$ is a Heaviside function and the retarded time t_r is found from solution of

$$t_r = t - \frac{1}{c}\sqrt{x^2 + y^2 + (z - vt_r)^2}, \tag{18}$$

which is found to be

$$t_r = \frac{t - Mz/c - \sqrt{(t - Mz/c)^2 - (1 - M^2)(t^2 - r^2/c^2)}}{(1 - M^2)}, \tag{19}$$

where $r = \sqrt{x^2 + y^2 + z^2}$ and the negative sign in the solution has been taken to give the correct expression for t_r in the limit where v approaches zero. Equation (4) gives the acoustic pressure as

$$p = \frac{\beta P_0}{4\pi C_P}\left\{\frac{v(z - vt)u(t_r)}{\left[(z - vt)^2 + (x^2 + y^2)(1 - v^2/c^2)\right]^{3/2}} + \frac{\partial t_r}{\partial t}\frac{\delta(t_r)}{\sqrt{(z - vt)^2 + (x^2 + y^2)(1 - v^2/c^2)}}\right\}, \tag{20}$$

where the derivative of the retarded time with respect to time from Eq. (18) is

$$\frac{\partial t_r}{\partial t} = \frac{1}{\left[1 - \frac{M(z - vt_r)}{\sqrt{x^2 + y^2 + (z - vt_r)^2}}\right]}. \tag{21}$$

The photoacoustic pressure from Eq. (20), as shown in Fig. 3, consists of two waves, the first of which, as described by the last term in Eq. (20), is a sharp, delta function compression propagating at a speed c arising from initiation of the source motion. This wave is followed by a compression and then immediately by a rarefaction traveling in the direction of motion of the source centered at the point $z = vt$. The pressure distribution along the source trajectory is shown in Fig. 3(b). Compared with the two-dimensional result, the pressure following the rarefaction peak vanishes rapidly with no trailing wave present. Such a waveform difference has its origin in the strikingly different characteristics of the two-dimensional and three-dimensional waves. For an impulsive source in space and time, the energy of the wave at time t in a three-dimensional geometry will be found within a thin spherical layer with the radius ct centered at the source point. The waveform is essentially a spherical delta function.

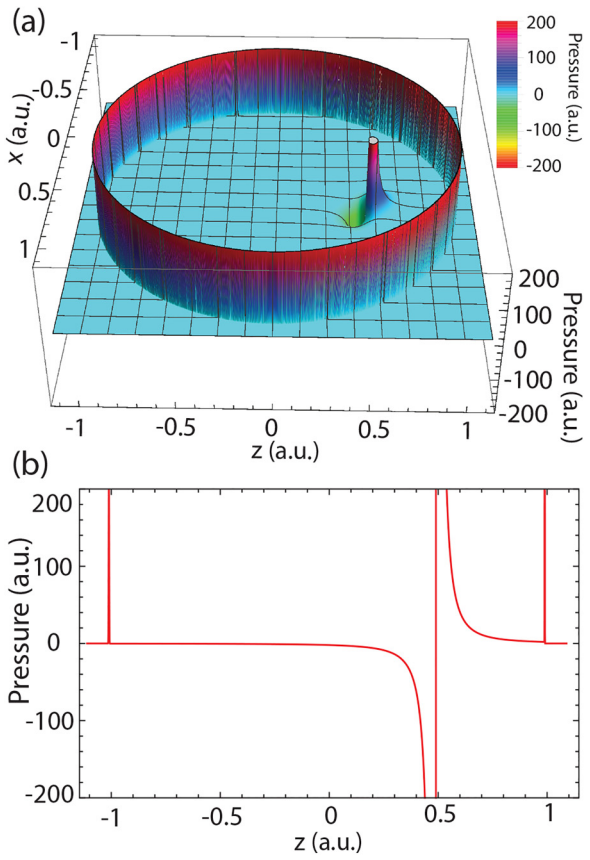

FIG. 3. Photoacoustic pressure from a delta function point source moving at half of the sound speed in a three dimensional geometry. (a) Distribution of the pressure on the xz plane with $y = 0$ at $t = 1$. The pressure is truncated to visualize the fine features of the wave within the causal region. (b) The pressure distribution along the z axis.

In the two-dimensional case, the energy of the cylindrical wave will spread from the periphery $R = ct$ to the source location.

In order to evaluate the amplification effect from speed matching in a three-dimensional geometry, a Gaussian source moving at the sound speed is considered. The heating function for the moving Gaussian source can be written as

$$H(\vec{\mathbf{r}}, t) = \frac{P_0}{(\sqrt{\pi}\sigma)^3}e^{-\frac{x^2 + y^2 + (z - vt)^2}{\sigma^2}}, \tag{22}$$

where v has been taken as c. It is clear that the maximum pressure occurs at the source position, the maximum pressure at this point being

$$p_{\max} = \frac{\beta P_0}{4\pi^{3/2}\sigma^2 C_p}\left[c\sqrt{\pi}\,\mathrm{erf}\left(\frac{2ct}{\sigma}\right) - \frac{1 - e^{-4c^2t^2/\sigma^2}}{t/\sigma}\right], \tag{23}$$

whose value is bounded by $\beta c P_0/(4\pi\sigma^2 C_p)$ as time approaches

infinity. Thus, the thermal expansion coefficient, the spatial width parameter, and the specific heat capacity are the physical quantities that limit the amplitude of the wave at long times. The finite result for the bound indicates that in the three-dimensional geometry, amplification of photoacoustic wave is limited, which can be ascribed to the strong spherical divergence. Note that a Taylor expansion of Eq. (23) around $t = 0$ can be carried out giving

$$p_{\max} = \frac{\beta P_0}{4\pi^{3/2}\sigma^2 C_p}\left[\frac{8c^4t^3}{3\sigma^3} - \frac{64c^6t^5}{15\sigma^5} + \frac{32c^8t^7}{7\sigma^7} + O(t^9)\right]. \quad (24)$$

The initial growth of the wave is governed by the dominant first term within the parenthesis which implies $t \ll \sigma/c$. This condition indicates that a larger spot permits a longer growth duration. However, as denoted in Eq. (23), the limiting pressure as time goes to infinity is inversely proportional to σ^2, which favors the use of a smaller spot. Thus, a smaller spot is generally preferred as it gives larger pressure within a short time period.

A comparison of the evolution of acoustic wave amplitude with time for different geometries is given in Fig. 4. It can be seen that the geometric divergence will compete with the sound amplification originating from speed matching in higher dimensions, resulting in a weakened or bounded amplification effect. Also note that in contrast with its electromagnetic counterpart, there remains technical challenges to realize experimentally a point photoacoustic source moving in space. The theoretical work presented here only provides a guidance on how the geometric divergence of acoustic waves in two and three dimensions will adversely affect the amplification effect enabled by the moving source effect.

It is also of interest to compare the photoacoustic waves from supersonic motion in two and three dimensions. Although the photoacoustic waves from a delta function source can be derived analytically, it is advantageous to calculate the responses from Gaussian sources here to avoid singularities that may obscure critical features of the waves. Two Gaussian heating functions as described in Eqs. (13) and (22) with $v > c$ are considered for the two and three-dimensional cases. The pressure distribution along the source trajectory is obtained through the use of a finite difference calculation. Several differences between the two and three-dimensional geometries can be seen in Fig. 5(b). First, within the Mach cone (region II), the photoacoustic pressure is zero in the two-dimensional geometry while it is negative for the three-dimensional case. Second, within the circular region I, the two-dimensional photoacoustic pressure shows a gradual change from compression to rarefaction along the x axis while the three-dimensional pressure remains zero in this region.

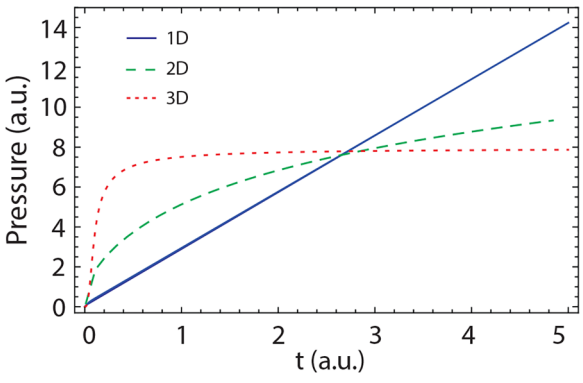

FIG. 4. Evolution of the maximum pressure with time when the source moves at the sound speed in different geometries Due to geometric divergence, the pressure grows more slowly as the dimensionality increases and is eventually bounded in the three-dimensional case. For the two and three dimensional cases, $\sigma = 0.1$. Parameters for the one dimensional result are the same as those used in Fig. 1.

IV. SUPERPOSITION OF SEQUENTIAL PULSES

It is intuitively clear that a continuous moving source can be regarded as the superposition of a series of spatially and

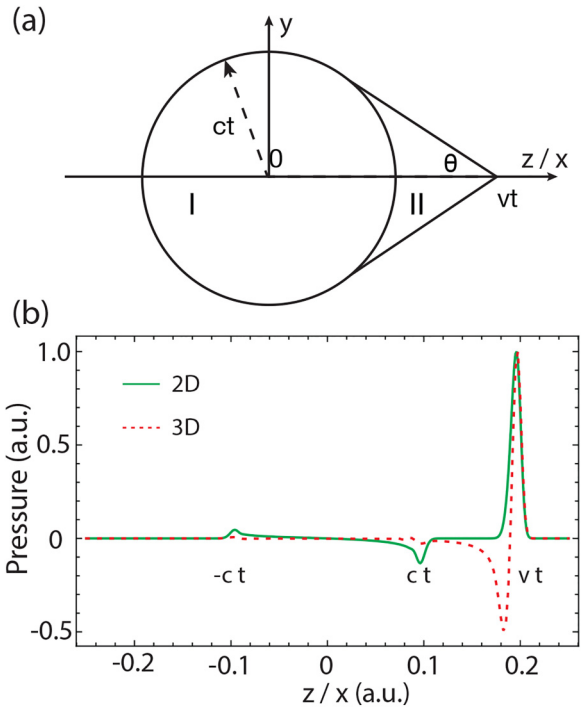

FIG. 5. Photoacoustic pressure from sources moving at a supersonic speed ($v = 1.5c$) in two and three dimensional geometries. (a) Diagram showing the regions where the pressure wave is confined. Region *I* corresponds to the ordinary causal region (bounded by $-ct$ to ct), while region *II* (which precedes ct) is a Mach cone unique to supersonic motion where θ is half of the vertex angle of the cone. (b) Pressure distribution along the source trajectory for a Gaussian source moving in two and three dimensional geometries with the heating functions described by Eqs. (13) and (22), respectively. The pressure magnitude is normalized by the maximum pressure in the plot.

temporally displaced pulses. Such an analogy indicates that although a continuous laser beam is used, every spatial point along the trajectory experiences a delayed pulsed excitation. When the source moves at the sound speed, the elementary waves emanating from individual pulses are coherently added at the wavefront, which qualitatively explains why the moving source could increase the pressure in the thermoelastic regime. In so far as experiments are concerned, this analogy implies that an appropriately delayed pulsed laser array can be used to amplify photoacoustic waves.

This process can be described quantitatively by assuming the source moves along the z axis, writing the moving part of the heating function as $h(z - vt)$, where v is the speed of the source. An expression for the motion function can be written in either of the two forms

$$\begin{aligned} h(z - vt) &= \int_0^Z h(z - z_0)\delta(z_0 - vt)dz_0 \\ &= \lim_{N\to\infty} \sum_{n=0}^{N-1} h(z - z_0^n)\delta(t - z_0^n/v)\Delta t_0, \end{aligned} \tag{25}$$

where Z and T are the spatial extension and the temporal duration of the excitation, N is the total number of pulses, $z_0^n = nv\Delta t_0$ and $\Delta t_0 = T/N$. The above summation describes the superposition of sources temporally displaced by Δt_0 and distributed in space by $v\Delta t_0$. The pressure wave p^n generated from the elementary excitation $H^n = h(z - z_0^n)\delta(t - z_0^n/v)\Delta t_0$ gives an approximate, overall pressure resulting from the moving source as

$$p_{sum} \approx \sum_{n=0}^{N-1} p^n, \tag{26}$$

the justification for which follows from the linearity of the wave equation for pressure. The application of the summation method to one and three-dimensional calculations where p^n can be obtained in a closed form for a static Gaussian source is given below.

A. One-dimensional geometry

As was shown in Ref. 30, the photoacoustic pressure for short pulsed excitation can be found as the mapping of the spatial distribution of the heating source, which obviates the need to solve the wave equation in order to obtain p^n. Suppose the heating function is of the form $H(z, t) = \bar{\alpha}F_0\hat{h}(\hat{z})\delta(t)$, where $\bar{\alpha}$ is the absorption coefficient, F_0 is the laser fluence, $\hat{h}$ is a dimensionless function describing the spatial part of H, and $\hat{z}$ is the coordinate scaled with the absorption length parameter ξ_0. The photoacoustic wave is a mapping of the spatial deposition of heat into the time dependence of the photoacoustic pressure according to

$$p(z, t) = \frac{\bar{\alpha}\beta F_0 c^2}{2C_P}\left\{\hat{h}\left[\frac{c(t - z/c)}{\xi_0}\right] + \hat{h}\left[\frac{c(t + z/c)}{\xi_0}\right]\right\}. \tag{27}$$

Here, $\hat{h}(\hat{z})$ is taken to be a dimensionless, normalized Gaussian function of the form $\hat{h}(\hat{z}) = 1/(\hat{\sigma}\sqrt{\pi})\exp\left[-\hat{z}^2/\hat{\sigma}^2\right]$, where $\hat{\sigma}$ is a dimensionless width parameter. The pressure from $n'th$ pulse can thus be written as

$$p^n = \frac{\bar{\alpha}\beta I_0 c^2 T}{2C_P N\hat{\sigma}\sqrt{\pi}}\left\{e^{-\left(\frac{c}{\xi_0\hat{\sigma}}\right)^2\left[(t - n\Delta t_0) - \left(\frac{z - n\Delta z_0}{c}\right)\right]^2} + e^{-\left(\frac{c}{\xi_0\hat{\sigma}}\right)^2\left[(t - n\Delta t_0) + \left(\frac{z - n\Delta z_0}{c}\right)\right]^2}\right\}.$$

The overall photoacoustic pressure for the moving source can then be approximated by summing p^n according to Eq. (26). It is found that in the limit where N is made infinite and the parameters $\hat{\sigma}$ and F_0 are taken to be $v\theta/\xi_0$ and I_0T/N, respectively, the summation becomes an integral, which upon evaluation gives Eq. (7) exactly.

B. Three-dimensional geometry

A similar procedure can be used in three dimensions given the solution for a static point source. An equivalent variant of Eq. (25) is given by

$$h(t - z/v) = \lim_{N\to\infty} v\sum_{n=0}^{N-1} h(t - t_0^n)\delta(z_0^n - z)\Delta t_0, \tag{28}$$

which decomposes the moving source into a series of elementary sources whose spatial part is a Dirac delta function.

The elementary sources can be taken to be a normalized Gaussian with a heating function given by

$$H(\mathbf{x}, t) = \frac{E_0}{\theta\sqrt{\pi}}e^{-(t - t_0)^2/\theta^2}\delta(x)\delta(y)\delta(z - z_0), \tag{29}$$

where E_0 is the absorbed pulsed energy and t_0 is the time when the optical power reaches its maximum. The resulting photoacoustic pressure within the causal sphere is found[31] to be

$$p = -\frac{\beta E_0}{4\pi\sqrt{\pi}C_P\theta^3}\frac{(t - t_0 - r/c)e^{-(t - t_0 - r/c)^2/\theta^2}}{r}, \tag{30}$$

where $r = \sqrt{x^2 + y^2 + (z - z_0)^2}$. Note that a compressive delta sphere which results from the abrupt initialization of the source at $t = 0$ is not included in the expression as it is not relevant to the Gaussian feature of the source. The delta waveform can also be naturally excluded by extending the time t to $-\infty$.

By replacing t_0 with $t_0^n = n\Delta t_0$, r with $r^n = \sqrt{x^2 + y^2 + (z - t_0^n v)^2}$, and $E_0 = P_0\Delta t_0$, Eq. (30) becomes the pressure from the nth pulsed excitation. Therefore, the total pressure can be approximated by

$$p_{sum} \approx -\frac{\beta P_0 T}{4\pi\sqrt{\pi}C_P\theta^3 N}\sum_{n=0}^{N-1}\frac{(t - t_0^n - r^n/c)}{r^n}\, e^{-(t - t_0^n - r^n/c)^2/\theta^2}. \tag{31}$$

Examination of Eq. (28) indicates that as N approaches the infinity, p_{sum} will converge identically to the pressure as found from a heating source of the form

$$H(x, y, z, t) = \frac{P_0}{\sqrt{\pi}v\theta}e^{-(z - vt)^2/(v\theta)^2}\delta(x)\delta(y). \tag{32}$$

It is thus clear that the summation method provides a flexible

approach to approximating the pressure waveform from a continuous moving source.

V. APPLICATION TO TRACE DETECTION

The fact that the photoacoustic pressure grows with time as the source moves at the sound speed has intriguing possibilities for its application in trace gas detection as a macroscopic, homogeneous gas medium permits the acoustic waves to be coherently added for an extended period, thus making full use of the amplification effect. Two different schemes have been recently reported which use either a sweeping laser beam or a moving optical grating for the purpose of speed matching. The resulting acoustic waves by these two methods are either broadband or monochromatic and can be categorized as time domain or frequency domain techniques.

A. Time domain technique

A time domain scheme, termed dynamic photoacoustic spectroscopy (DPAS), has been developed by the Lincoln Laboratory at Massachusetts Institute of Technology for remote detection of gases or aerosols.[32–34] As shown in Fig. 6(a), a continuous CO_2 laser beam with either constant or modulated intensity is swept by a spinning mirror and directed into the field of interest, resulting in acoustic waves detected by a broadband microphone or a laser vibrometer. At the radius where the linear velocity of the laser beam matches the sound speed, the acoustic waves are coherently added and a bipolar asymmetric wave is developed. For a laser traveling distance (integration path length) of approximately 0.6 m, the bipolar wave has a characteristic time scale on the order of 100 μs whose frequency components are in the audible range. Additionally, it was found that the performance of the system is insensitive to the chopping frequency, which affirms that a moving laser beam alone can excite photoacoustic waves.

It can be seen from Fig. 6(b) that the peak-to-peak amplitude of the acoustic waves shows a resonant dependence on the speed of sweeping—the amplitude reaches its maximum when the laser moves at the sound speed. Additionally, as shown in the inset of Fig. 6(b), the signal is proportional to the integration path length of the laser beam until the effects of geometric divergence, acoustic nonlinearities, or other energy dissipation paths become significant.

For the objective of stand-off detection, the use of acoustic resonators and the frequency-domain modulation technique, as commonly adopted in photoacoustic trace detection, is largely prohibited, which poses additional challenges for photoacoustic sensing. DPAS overcomes this difficulty by taking advantage of the moving source effect. It was found from the experiment that the photoacoustic energy conversion efficiency was increased from the typical 10^{-12} to 10^{-8} by the speed matching condition, which substantially improved the signal-to-noise ratio. For sulfur hexafluoride (SF_6) detection with the microphone centered in a 9 in. diameter parabolic reflector, a clutter-limited sensitivity of 100 parts-per-trillion (ppt) has been predicted for a detection

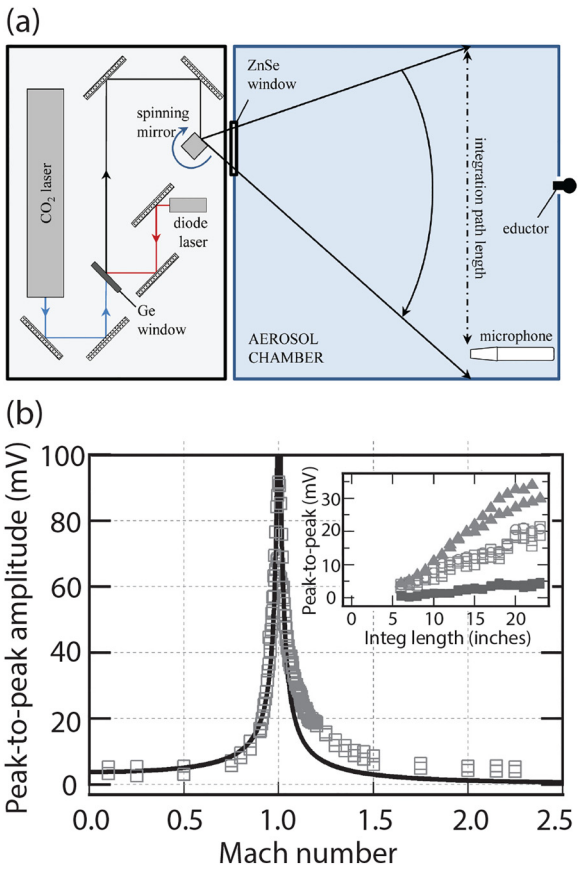

FIG. 6. (a) Experimental setup for the DPAS technique. A continuous CO_2 laser is swept using either a spinning mirror or cube. The laser beam can be optionally chopped by an optical chopper (not depicted) before entering the field of interest. An omnidirectional broadband microphone is placed near the radius where the linear velocity of the laser beam matches the sound speed. Alternatively, a laser vibrometer can be used which is better suited for the purpose of remote detection. A diode laser colinear with the CO_2 laser is added to facilitate alignment. Reproduced with permission from Sullenberger *et al.*, Optics Express **22**, A1810 (2014). Copyright 2014 OSA Publishing. (b) Dependence of the peak-to-peak signal on the moving speed of the laser beam, which can be varied by changing the angular frequency of the spinning mirror, with the microphone fixed in space. The solid curve is a fitted result based on a simple monopole radiator model. Inset: the peak-to-peak signal versus the integration path length of the laser beam. The laser power was 7 W and the rotation frequency of the mirror varied from 0 to 50 Hz. Green triangles: 15 ppm, cw; red open circles: 15 ppm, 3.1 kHz chopping; blue squares: 3.5 ppm, 3.1 kHz chopping. Reproduced with permission from Wynn *et al.* Applied Physics Letters **101**, 184103 (2012). Copyright 2012 AIP Publishing LLC.

range of approximately 2.7 m, an integration path length of 0.43 m, an interrogation time of 1.8 s, and a laser power of 3.5 W.[32] Using the same setup, the detection of gaseous ammonia (NH_3) has been demonstrated as well. By appropriate scaling and extrapolation, the sensitivity for NH_3 with a detection range of around 4.6 m is approximately 2 parts-per-billion (ppb).[32] For the detection of trace silica aerogel with diameters

between 0.39 and 0.68 μm, a sensitivity of approximately 500 particles/ml has been found for an interrogation time of 1 s and a laser power of 5 W.

B. Frequency domain technique

Another scheme that combines the moving source effect with the advantages of resonant detection has been reported as well.[35] This method is based on generating an optical grating moving in one direction in a short, longitudinal resonator so that the source motion speed matches the sound speed in the resonator. The resonator consists of a movable reflector at one end of the detection cell and a resonant piezoelectric crystal at the other end so that two additional resonance can be achieved: first, the length of the resonator can be adjusted to give a longitudinal resonance; second, the frequency of the grating can be made to match the resonance frequency of the piezoelectric crystal.

It is well known that when two phase coherent beams intersect at an angle, a grating is formed where the intensity of the combined beams at their point of intersection[36] is

$$I(\mathbf{x}, t) = I_0[1 + \cos(\mathbf{q}\cdot\mathbf{x} - \Omega t)], \tag{33}$$

where $\mathbf{q}$ is a difference wave vector given by $\mathbf{q} = \mathbf{k}_1 - \mathbf{k}_2$, where $\mathbf{k}_1$ and $\mathbf{k}_2$ are the propagation vectors for the two beams, and the frequency of the moving grating Ω is given by $\Omega = \omega_1 - \omega_2$, where ω_1 and ω_2 are the frequencies of the beams. Equation (33) describes a grating oscillating at a given point in space at a frequency Ω with a fringe spacing Λ given by

$$\Lambda = \frac{\lambda}{2\sin(\theta/2)}, \tag{34}$$

where λ is the wavelength of the laser beam and θ is the intersection angle between the two beams. Here, $\mathbf{q}$ is taken to be along the symmetry axis of the resonator designated as the z axis. In the trace detection experiments, the speed of the grating is matched to the sound speed by carefully adjusting the crossing angle θ between two incident beams so that $\Omega\Lambda = 2\pi c$.

The heating function for the wave equation for the moving grating is $H(\mathbf{x}, t) = \bar{\alpha} I(\mathbf{x}, t)$, where $\bar{\alpha}$ is the infrared optical absorption coefficient of the trace gas. The solution to the wave equation for pressure can be obtained by Fourier transformation of the time variable to give a Helmholtz equation whose solution, in turn, is found using a Green's function for the space variable. The photoacoustic pressure, when simplified to show only the resonance terms,[35] is found to be

$$p_{res} = \frac{\bar{\alpha}\beta I_0 \Omega}{C_p}\sum_{n=1}^{\infty}\frac{\cos k_n z}{[(\frac{\Omega}{c})^2 - (\frac{n\pi}{L})^2]}\left\{\frac{\sin[(k_n - q)L]}{(k_n - q)L}\sin(\Omega t) - \frac{\cos[(k_n - q)L] - 1}{(k_n - q)L}\cos(\Omega t)\right\}, \tag{35}$$

where L is the length of the resonator.

It can be seen from Eq. (35) that there are amplitude maxima in the photoacoustic pressure, when $\Omega/c = n\pi/L$ and $k_n L = qL$. These conditions correspond to a match between the frequency and wavelength of the grating so that $\Omega\Lambda = 2\pi c$ and that the resonator be an integral number of half wavelengths of the grating. Note that acoustic attenuation or diffraction, which limits the amplitude of p on resonance, is not included in the derivation.

The experimental apparatus used to generate the grating is shown in Fig. 7(a). A 10.6 μm beam from a continuous CO_2 laser was directed into two acousto-optic light modulators which gave steady beams shifted by approximately 40 MHz, the nominal driving frequency of the acousto-optic modulator. In the experiments, the two carrier frequencies fed into the light modulators were scanned slightly from this figure so that the

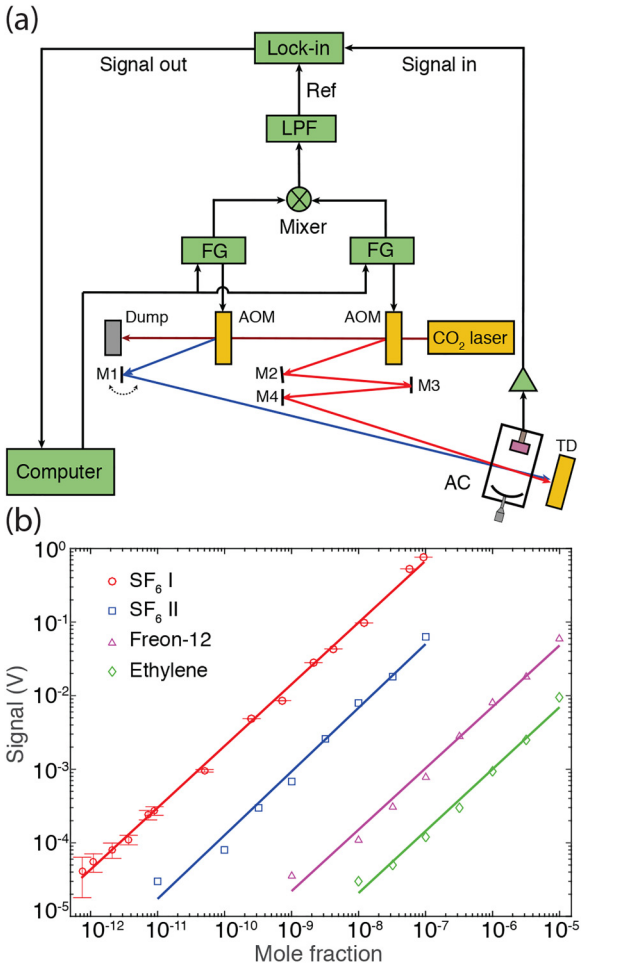

FIG. 7. (a) Experimental setup for the frequency domain technique which uses an infrared optical grating for the purpose of speed matching; (b) transducer voltage signal versus the concentration of different gases for two kinds of piezoelectric transducers. SF_6 I was detected by the α-BiB_3O_6 crystal while the other three samples were measured by the $LiNbO_3$ crystal. Reproduced with permission from Xiong *et al.*, Proc. Natl. Acad. Sci. **114**, 7246 (2017). Copyright 2017 National Academy of Sciences.

difference between the frequencies matched the resonant frequency of the transducer, which is on the order of 400 kHz.

The deflected beams from the light modulators were directed into a cell equipped at one end with a metal (either plane or concave) reflector whose position at one end of the cavity could be varied and a piezoelectric crystal fixed at the other end. The power of the beams entering the resonator was set to be 1 W. The reference for the radio frequency lock-in amplifier was generated by sending signals from the two function generators into a radio frequency mixer, the output from which was fed to a low pass filter set to pass the difference frequency at the resonance frequency of the detector crystal. The signal from the transducer was fed to a high input impedance, low noise amplifier followed by a second amplifier whose output was sent to a lock-in amplifier with a time constant of 1 s and a filter slope of 6 dB/oct.

Two different transducers were used in the experiments. In the first experiment, the transducer was a $LiNbO_3$ crystal 11.7 mm in diameter and 4.6 mm thick mounted in a housing with three set screws whose tips were ground to sharp points in an arrangement where the transducer was supported at its center. The quality factor (Q) of the $LiNbO_3$ transducer, determined by scanning the frequency of the grating, was measured to be 5800. The photoacoustic cell was equipped with an injection port at the top for addition of gases. Gas mixtures were made up barometrically using high purity SF_6, N_2, or Ar and stored in stainless steel gas tanks. Gas samples were injected into the photoacoustic cell operated at 1 atm with a hypodermic syringe. A plot of output signal versus mole fraction for three gases that absorb at 10.6 μm is shown in Fig. 7(b). The detection limit of SF_6 in N_2 using the $LiNbO_3$ crystal was found to be 10 ppt.

For the experiments with SF_6 in Ar, a specially fabricated α-BiB_3O_6 crystal with a resonance frequency of 443.15 kHz, a Q of 10 800 and a piezoelectric coefficient on the order of 40 pC/N was used. As shown in Fig. 7(b), a detection limit of 750 parts-per-quadrillion (ppq) of SF_6 in ultrapure Ar was found, which corresponds to an absorption coefficient of 8.1×10^{-11} cm^{-1} under the experimental conditions described above.

In the trace gas detection experiments, the crystal exhibits extremely small strains so that linear response over a large range of concentrations is guaranteed. It is noteworthy that the small signal generated in the infrared transmitting windows of a conventional photoacoustic cell which typically limits detection sensitivity is not found with the moving grating configuration since the speed matching condition is not satisfied in the window, in which sound travels much faster. In fact, the detection cell used in the trace detection experiments requires only two surfaces, the piezoelectric transducer and the hard reflector. The cavity need not be enclosed and does not require windows: given the short wavelength of the acoustic waves and the relatively large dimensions of the reflector and transducer, the resonator resembles a conventional plane parallel or hemispherical laser resonator. It was found as well that there was no measurable acoustic or electromagnetic pickup at the high frequency employed so that the device can be used for continuous *in situ* gas monitoring.

VI. CONCLUSIONS AND OUTLOOK

It is of note that the d'Alembert operator is found in the scalar wave equation in the electromagnetic theory as well as for the photoacoustic effect. That new solutions to the wave equation[30,37] have been found for the photoacoustic effect, despite the intense investigation of electromagnetic theory over the last century, is a consequence of the fact that monopole radiation is naturally generated photoacoustically by, for instance, pulsed heat deposition, while, on the other hand, the equivalent generation of electromagnetic monopole radiation would require the rapid creation of a single polarity charge—a generally impossible task. In so far as moving sources are concerned, again there are profound differences for the generation of outgoing waves between electromagnetic theory and photoacoustics. In the former, a uniformly moving charge in a vacuum does not give rise to outgoing waves, but carries with it only its static electric field translated in space. In photoacoustics, as has been shown here, uniform motion of an optical source produces a myriad of outgoing traveling acoustic waves.

The unbounded amplification effect described for a light source moving at the sound speed is unique to waves in one dimension. The reason the amplification is unbounded in one dimension is that only in this case is there confinement of the pressure in the wave; in two or three dimensions, there is a pressure increase that is synchronous with the source; however, owing to the geometry of the motion, pressure relief is possible in directions orthogonal to the motion, thus limiting any amplification at long times.

It is unfortunate that little experimental work has been published on moving photoacoustic sources. The production of a moving point source presents significant technical difficulties, although a method based on two-photon absorption might provide an approximation to a small volume source. Even the experiments reported here for motion in one dimension do not address directly the question of quantitative agreement between the theory and the experiment. An experiment with a line source in a two-dimensional geometry using a translating laser beam would perhaps be straightforward; however, recording the acoustic waveform would entail the use of an array of wideband microphones.

In so far as future applications of the technology described here is concerned, it is clear that the use of resonant piezoelectric transducers for trace gas detection shows great promise. In addition to the design of a photoacoustic detector based on a resonant tuning fork[7] and that described here where a solid crystal transducer was employed, it can be expected that the use of multiple, evenly spaced infrared beams directed perpendicularly to the axis of the resonator can be used to excite a piezoelectric transducer in a longitudinal resonator, as is described above. Such a design would simulate the effect of a moving grating, giving amplification of the acoustic wave each time a crest in the acoustic wave passes

through one of the beams in the array-provided, of course, that the repetition rate of the laser is correctly synchronized with the acoustic wave motion. Such a configuration using short pulses would act as synchronized Dirac combs and would constitute a time domain version of the experiment reported in Ref. 35, presumably achieving a similar high sensitivity for trace gas detection.

The versatility of controlling optical radiation offers a broad platform for generating sound waves with widely differing characteristics through the photoacoustic effect. By changing the spatial or temporal profiles of the optical radiation, sound waves with controlled amplitude, temporal behavior, frequency spectra, and spatial distribution (directionality) can be generated. The moving source effect represents a typical example of taking advantage of the controllability of the laser beam. Although not discussed here, more complex moving patterns generated from laser beam motion in space, such as oscillation or circular motion, can be achieved with little difficulty giving rise to unique acoustic wave patterns virtually impossible to create using conventional acoustic transducers.

ACKNOWLEDGMENTS

The authors are grateful to the U.S. Department of Energy under Grant No. DE-SC0001082 for support of this research and also to Parallax Technology, Inc. for donation of the CO_2 laser for the experiment.

REFERENCES

[1]A. G. Bell, J. Soc. Telegraph Eng. **9**, 404 (1880).
[2]A. Rosencwaig, *Photoacoustics and Photoacoustic Spectroscopy* (Wiley, New York, 1980).
[3]J. Hodgkinson and R. P. Tatam, Meas. Sci. Technol. **24**, 012004/63 (2013).
[4]M. W. Sigrist, "Air monitoring, optical spectroscopic methods," in *Encyclopedia of Environmental Analysis and Remediation* (John Wiley, 1998), pp. 84–116.
[5]A. Karbach and P. Hess, J. Chem. Phys. **83**, 1075 (1985).
[6]A. Karbach and P. Hess, J. Chem. Phys. **84**, 2945 (1986).
[7]H. Zheng, L. Dong, A. Sampaolo, H. Wu, P. Patmisco, X. Yin, W. Ma, L. Zhang, W. Yin, V. Spagnolo, S. Jia, and F. K. Tittel, Optics Lett. **41**, 978 (2016).
[8]A. Miklos, C.-H. Lim, W.-W. Hsiang, G.-C. Liang, A. H. Kung, A. Schmohl, and P. Hess, Appl. Opt. **41**, 2985 (2002).
[9]C. K. N. Patel and A. C. Tam, Rev. Modern Phys. **53**, 517 (1981).
[10]A. C. Tam, Rev. Modern Phys. **58**, 381 (1986).
[11]*Photoacoustic Imaging and Spectroscopy*, edited by L. V. Wang (CRC Press, Boca Raton, 2009).
[12]A. I. Bozhkov and F. V. Bunkin, Sov. J. Quantum Electron. **5**, 956 (1976).
[13]A. I. Bozhkov, F. V. Bunkin, I. B. Esipov, A. I. Malyarovskii, and V. G. Mikhalevich, Sov. Phys. Acoust. **26**, 100 (1980).
[14]A. I. Bozhkov, F. Bunkin, and A. A. Kolomenskii, Sov. J. Quantum Electron. **7**, 536 (1977).
[15]A. I. Bozhkov and A. A. Kolomenskii, Sov. J. Quantum Electron. **8**, 1449 (1978).
[16]F. V. Bunkin, A. I. Malyarovskii, V. G. Mikhalevich, and G. P. Shipulo, Sov. J. Quantum Electron. **8**, 270 (1978).
[17]A. D. Pierce and Y. H. Berthelot, J. Acoust. Soc. Am. **83**, 914 (1988).
[18]A. A. Zaitsev, Sov. Phys. Acoust. **19**, 234 (1973).
[19]V. N. Lugovoi and V. N. Strel'tsov, Sov. Phys. JETP **38**, 701 (1974).
[20]F. V. Bunkin, V. G. Mikhalevich, and G. P. Shipulo, Sov. J. Quantum Electron. **6**, 238 (1976).
[21]A. I. Bozhkov, F. V. Bunkin and A. A. Kolomenskii, Sov. Tech. Phys. Lett. **4**, 516 (1978).
[22]W. Bai and G. J. Diebold, Phys. Rev. E **98**, 032125 (2018).
[23]S. Temkin, *Elements of Acoustics* (John Wiley, New York, 1981).
[24]W. Bai and G. J. Diebold, Int. J. Thermophys. **37**, 1 (2016).
[25]V. S. Vladimirov, *A Collection of Problems on the Equations of Mathematical Physics* (Springer-Verlag, Berlin, 1986).
[26]V. E. Gusev and A. A. Karabutov, *Laser Optoacoustics* (American Institute of Physics, New York, 1993).
[27]L. D. Landau and E. M. Lifshitz, *Fluid Dynamics*, 2nd ed. (Pergamon, New York, 1987), see Section 71
[28]J. Matthews and R. L. Walker, *Mathematical Methods of Physics*, 2nd ed. (Benjamin Cummings, Menlow Park, 1970), see Section 9-4
[29]D. Griffiths, *Introduction to Electrodynamics* (Prentice Hall, Englewood Cliffs, 1981).
[30]G. J. Diebold, T. Sun, and M. I. Khan, Phys. Rev. Lett. **67**, 3384 (1991).
[31]W. Bai and G. J. Diebold, J. Acoust. Soc. Am. **142**, 3796 (2017).
[32]C. M. Wynn, S. T. Palmacci, M. L. Clark, and R. R. Kunz, Opt. Eng. **53**, 021103 (2013).
[33]C. M. Wynn, S. Palmacci, M. Clark, and R. Kunz, Appl. Phys. Lett. **101**, 184103 (2012).
[34]R. Sullenberger, M. Clark, R. Kunz, A. Samuels, D. Emge, M. Ellzy, and C. Wynn, Opt. Express **22**, A1810 (2014).
[35]L. Xiong, W. Bai, F. Chen, X. Zhao, F. Yu, and G. J. Diebold, Proc. Natl. Acad. Sci. **114**, 7246 (2017).
[36]H. J. Eichler, P. Gunter, and K. W. Pohl, *Laser-Induced Dynamic Gratings* (Springer, Berlin, 1985).
[37]G. J. Diebold, M. I. Khan, and S. M. Park, Science **250**, 101 (1990).